43rd Turbomachinery & 30th Pump Users Symposia (Pump & Turbo 2014)
September 23-25, 2014 | Houston, TX | pumpturbo.tamu.edu

COMPUTATIONAL INVESTIGATION OF COUPLING GUARD HEATING AND MITIGATION

Vishal Jariwala
Aerodynamics Engineer
Elliott Group
Jeannette, Pennsylvania, USA
vjariwal@elliott-turbo.com

Daryll Turner
Senior Consulting Engineer
Elliott Group
Jeannette, Pennsylvania, USA
dturner@elliott-turbo.com

James Hardin
Senior Engineer
Elliott Group
Jeannette, Pennsylvania, USA
jhardin@elliott-turbo.com

Vishal Jariwala is an Aerodynamics Engineer in Research and Development at Elliott Group, Jeannette, PA. He designs centrifugal compressor stages using analytical methods including computational fluid dynamics (CFD). His experience also includes centrifugal compressor prototype testing, CFD algorithm development, and software development. He is interested anything related to aerodynamics as well as novel applications of sensors. He holds a Master's degree in Aerospace Engineering from The University of Michigan – Ann Arbor, and a Bachelor's in Mechanical Engineering from Regional Engineering College, Surat, India. In Pennsylvania, he has obtained Engineering-in-Training (EIT) certification. Vishal is an avid radio-controlled aircraft flyer and a General-class amateur radio operator.

James Hardin is a Senior Engineer in the Research and Development at Elliott Group, in Jeannette, Pennsylvania, where he performs computational fluid dynamics (CFD) and other aerodynamic analyses for turbines and compressors. Previous experience includes CFD and other analyses on shipboard propulsion and piping systems with Westinghouse Electric Corporation, and turbine design support and testing at Elliott Company. He has 33 years of engineering experience, mostly in aerodynamics and fluid systems.

Mr. Hardin received a B.S. degree (Mechanical Engineering, 1981) from Carnegie-Mellon University, and is a registered Professional Engineer in the State of Pennsylvania.

Daryll began working at Elliott Company in Jeannette, PA in 1975. He joined CITGO Refining in 1987 as rotating equipment engineer. In 1991 he helped form an international power recovery expander Users group. Daryll joined Saudi Aramco's Consulting Services Department in Dhahran, Saudi Arabia in 1991 becoming rotating equipment specialist providing technical support to Saudi Aramco operating facilities and projects. He served as program chairman for the Saudi Arabian Eastern Province chapter of the ASME. He joined Dresser-Rand in Olean, NY in 1998 working in the axial compressor and power recovery expander group. Daryll returned to Elliott Co. in 2000 where he now works as senior consulting engineer for power recovery expanders. Daryll graduated from Carnegie Mellon University in 1975 with a BSME, is a member of ASME, coauthored and presented the short course Introduction to Steam Turbines, and coauthored a paper on using at speed balance machines to assess and improve rotor and bearing system stability.

ABSTRACT

High coupling guard temperature and oil misting on a power recovery expander led to a computational fluid dynamics (CFD) investigation of air flow and heat transfer in the coupling guard. The analyses included full 360-degree geometry, varying inlet and outlet configurations, different exhaust pressures, and both including and neglecting the flange bolt heads. With bolt heads included, the predicted coupling guard surface temperatures approximately matched values measured in the field. In the particular field problem addressed here, the measured temperatures were 219 to 222°F (104-106°C), while the CFD predicted temperature ranged from 209-227°F (98-108°C).

Among the important findings are:

- The moving bolt heads generate much of the heat in a coupling guard.
- Properly placed outlet ports can use the bolt heads as a blower, increasing air flow through the coupling guard and lowering the temperature.
- Small reductions in exhaust pressure can lower the coupling guard surface temperature significantly.

Numerous plots, graphs, and tables give insight into the flow field inside the coupling guard. These analyses can guide the design of coupling guards with lower surface temperatures.

INTRODUCTION

Up to the middle 1970s, lubricated gear type couplings (either grease packed or continuous oil lubrication type) were the norm in the refining and petrochemical industry. Totally enclosed guards for these couplings were simple structures with two major concerns: proper drainage of oil and prevention of oil leakage.

Later, dry couplings began gaining acceptance. By eliminating gears, they eliminated tooth wear and the potential vibration caused by them, as well as the need for an oil lubrication system. They also reduced thrust bearing loading.

Dry couplings also need guards for safety reasons. Equipment and coupling manufacturers, however, quickly learned that coupling guard design was an important issue with dry couplings. Dry couplings generally had larger flange diameters than gear couplings of comparable power capacity. The larger coupling flanges with higher number of bolt heads caused significant amounts of windage, resulting in frictional heating of the air in the coupling guard. Coupling guard volume, net cooling air flow, and clearance between the flanges and the guard internal wall became important factors.

An improperly designed coupling guard results in unacceptably high coupling guard surface and internal coupling temperatures. Further, close radial clearances effectively create separated "hot" volumes inside the guard.

Several papers have been presented at the Texas A&M Turbomachinery Symposium over the years discussing coupling guard design issues (Calistrat and Munyon (1985), Calistrat (1990), and Carter et al. (1994)). These references provide good information, but there is still a need for definitive guidelines covering all aspects of coupling guard design. Coupling manufactures do provide coupling guard temperature prediction software, but these programs do not address details of coupling guard design such as location and number of inlet breathers, interior baffle design, and location and number of outlets. Such details are important to meet the API 671 requirement that guard temperature should not exceed 160°F (70°C) (API 2007).

High speed coupling guard temperature and oil misting were experienced during commissioning of an equipment string consisting of a 32 MW FCC power recovery expander, reducing gear, and synchronous generator at a US Gulf coast refinery. After about six hours of continuous operation at normal speed (3600 RPM), significant oil misting was observed from the high speed coupling guard breather vent. The coupling guard is shown in Figures 1-3.

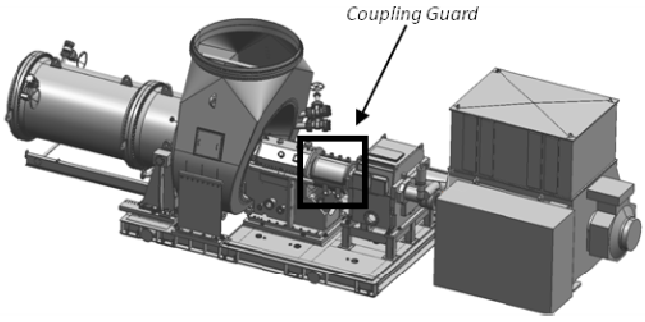

Figure 1. Coupling Guard on a Turbo Expander.

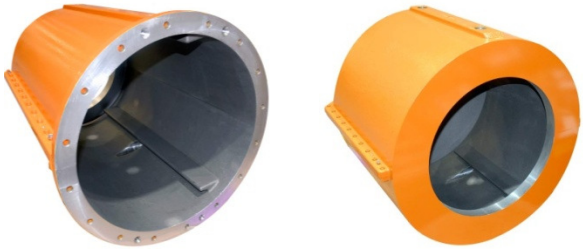

Figure 2. Coupling Guard (Two Different Views).

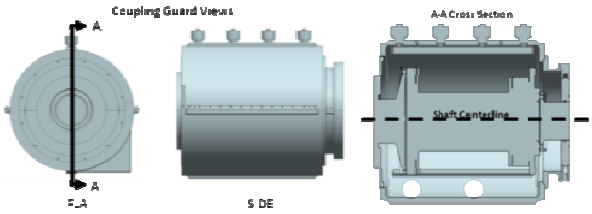

Figure 3. Coupling Guard (Cross Section).

The coupling guard included four 1-1/2-inch (38-mm) top-mounted inlet air breathers and a single off-center tangentially oriented 4-inch (102-mm) combined drain and vent. An axially oriented baffle inside the top half coupling guard was positioned to draw in fresh air through the four top mounted breathers. A second axially oriented baffle was positioned to collect air circulating in the direction of rotation and discharge it to the combination vent and drain.

Because of the oil misting, a low pressure loss coalescing filter was installed on the coupling guard combined vent and drain. The vent piping area was increased by connecting a second 4-inch tangentially oriented vent at the axial center of the coupling guard (Fig. 4). The two 4-inch (102-mm) vents were connected together into a single 6-inch (152-mm) vent pipe that ran vertically to the 6-inch (152-mm) inlet coalescing air filter (not shown). The additional vent was intended to

increase air flow through the coupling guard to help reduce the coupling guard temperature which was believed to be contributing to the oil misting.

A temperature survey of the coupling guard upper half surface and the gas exiting the coupling guard vent was made as a part of the troubleshooting process. With the single 4-inch (102-mm) breather vent, the exterior surface of the guard varied from 219°F (104°C) to 222°F (106°C). Gas exiting the breather was hotter than 220°F (104°C). The additional central 4-inch (102-mm) tangential vent reduced coupling guard exterior temperature to 197-203°F (92-95°C). No gas exit temperature was available for the modified configuration.

The temperature of the top center section of the coupling guard was 197°F (92°C). The gear end of the coupling guard, the end with the 4-inch (102 mm) tangential vent located closest to the coupling flange, was operating at 200°F (93°C); and the opposite end closest to the expander and furthest from a vent was operating at 203°F (95°C).

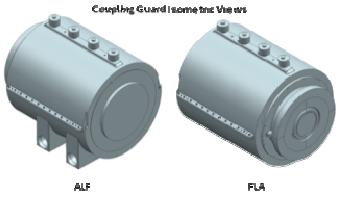

Figure 4. Coupling Guard with Two Outlets.

Adding the coalescing filter eliminated the oil misting from the coupling guard, but the guard temperature remained higher than desirable. None of the existing references or coupling guard temperature prediction software specified how much air flow would be necessary to reduce coupling guard temperature to acceptable values. Consequently, we undertook computational fluid dynamics (CFD) simulations of the coupling guard to understand the effects of changes in geometry and outlet pressure on coupling guard temperature.

CFD MODEL SETUP WITHOUT BOLTS

Two sets of CFD models were built with one major difference: whether the bolt heads in the coupling flanges were included or not. The moving bolt heads impart energy to the air, increasing temperature, and may act as a rudimentary pump to increase mass flow, possibly reducing temperature. Without the bolt heads, the only sources of heat are the hot shaft surface and small skin friction heating. In a way, the case without bolt heads simulates a "perfect" bolt-head windage reduction feature. It shows the extreme limit of what effects might be possible by reducing bolt-head windage.

We began with the simpler model, without bolt heads. Because of the lack of symmetry, a 360-degree representation of the fluid and solid domains was created, unlike the CFD analyses reported in Pennington and Meck (2012). The fluid domain was further simplified by eliminating bolt holes and platforms in the solid domain and small gaps from the shaft. The first CFD model is shown in Figures 5 and 6.

To facilitate future geometry changes, the fluid and solid domains were split into four parts. The inlets and outlets occupied their own sectors, while the remaining fluid and solid regions composed the other sectors. The splits in the solid domain matched the locations of those in the fluid domain. Extensions were added to the inlet and outlet faces to move boundary conditions away from the regions of interest.

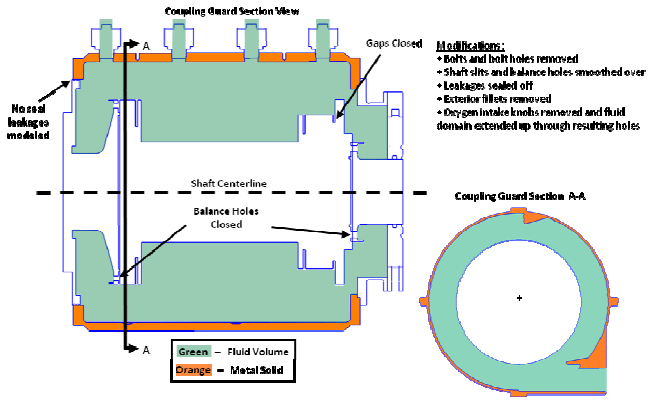

Figure 5. CFD Model without Bolts.

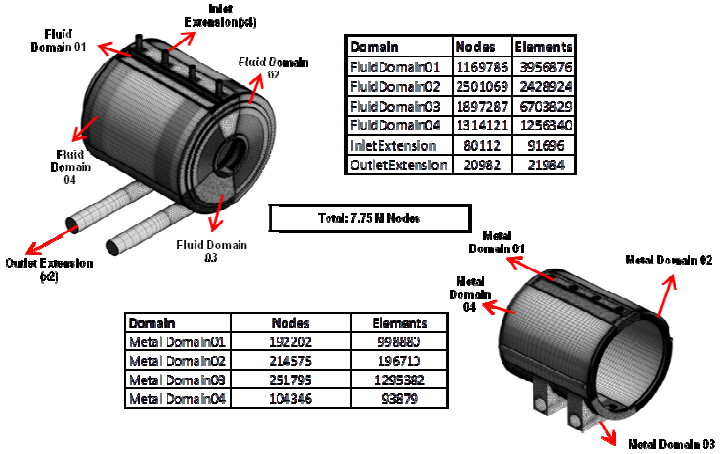

Domain	Nodes	Elements
FluidDomain01	1169785	3956876
FluidDomain02	2501069	2428924
FluidDomain03	1897287	6703829
FluidDomain04	1314121	1256340
InletExtension	80112	91696
OutletExtension	20982	21984

Domain	Nodes	Elements
Metal Domain01	192202	998880
Metal Domain02	214575	196710
Metal Domain03	251795	1295382
Metal Domain04	104346	93879

Figure 6. Domain and Mesh Setup – Model without Bolts.

A hybrid tetrahedral/prism mesh was employed for the inlet and outlet domains (both solid and fluid), with prisms near the wall to capture the boundary layer. Hexahedral mesh was used for all other sectors and extensions. Total mesh size was approximately 7.75 million nodes with individual domain sizes shown in Figure 6. All fluid domains were meshed for wall integration analysis (Y+ < 1) using near-wall spacing of 1.5×10^{-4} inch (0.0038 mm).

Steady-state flow analyses with conjugate heat transfer were carried out using the commercial CFD program ANSYS CFX, version 13 [CFX is a registered trademark of ANSYS, Inc.]. The SST turbulence model with reattachment modification was used. The cases without bolts are listed in Table 1.

Table 1. Cases Analyzed for Boltless Model.

Case #	Exit Pressure (psi)	Open Outlets	Inlet P (psi)	Inlet T (°F)
1	14.7	Central, End	14.7	95
2	14.6	Central, End	14.7	95
3	14.8	Central, End	14.7	95
4	14.7	End	14.7	95

Cases 1 through 3 included both outlets as they were installed in the field after modifications. Case 4 went back to the original configuration after results from the first cases, discussed below, indicated that the central outlet could ingest air. The exit pressure for cases 1 and 4 was chosen to approximate a low-loss discharge to atmosphere. Cases 2 and 3 were intended to evaluate the sensitivity of results to the exit pressure. Case 3 was of particular interest to evaluate the effect of backpressure from the coalescing filter. We wanted to know whether the motion of the rotating shaft would be enough to overcome the backpressure even though it was higher than the inlet pressure.

The details of the fluid boundary conditions are provided in Figures 7 and 8. The outlets were modeled as "opening" boundary conditions in CFX. This boundary condition allows flow to enter or leave the model. The specified pressure is treated as static if the flow direction is out of the domain and as total if the direction is into the domain. The total temperature was set to 95°F (35°C) for ingestion. While ingestion through the exhaust pipe is possible, this boundary condition may enforce unrealistically cool flow into the system. To understand this better, a case (Case 4) with the central outlet pipe walled off was included.

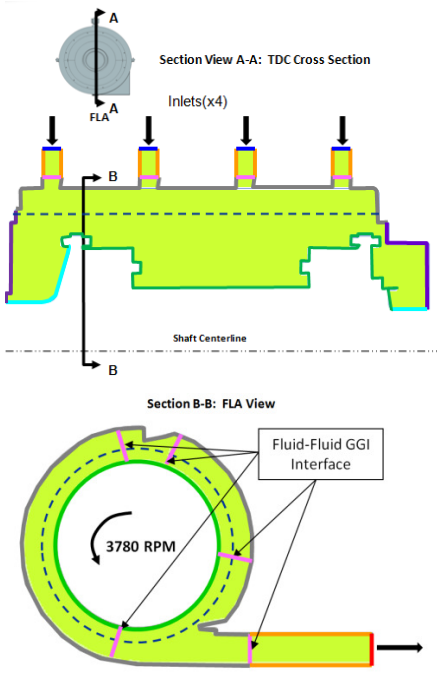

Figure 7. Coupling Guard Fluid Domain Boundary Conditions.

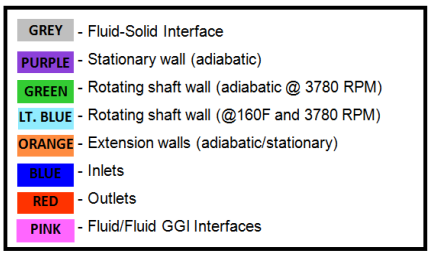

Figure 8. Boundary Conditions Guide (Applicable to Figure 7).

All walls in the fluid domain were considered adiabatic except those at the ends of the rotating shaft, which were fixed at 160°F (71°C), and the outer coupling guard surface, through which heat transfer was calculated. All rotating shaft walls were set to 3780 RPM.

The coupling guard metal domain was considered to be solid aluminum with all walls being stationary, and the external walls exposed to the same near ambient conditions as the inlets. A heat transfer coefficient modeling free convection off of a cylinder in quiescent air was implemented to account for heat loss to the environment (Equation (1)).

$$\mathrm{HTC} = 0.27\left[\frac{\mathrm{BTU}}{\mathrm{hr}\cdot\mathrm{ft}^{7/4}\cdot\mathrm{F}^{5/4}}\right]\times\left(\frac{T_{Wall}[\mathrm{F}]-T_{Ambient}[\mathrm{F}]}{\mathrm{Diameter}[\mathrm{ft}]}\right)^{1/4}$$

Equation 1. Heat Transfer Coefficient.

Other walls in the solid domain contact other casing components that were not modeled here and were treated as adiabatic. Fluid-fluid and solid-solid interfaces were set as General Grid Interfaces (GGI's)which allow different mesh structures to be connected. Figures 9 and 10 show the locations of solid boundary conditions and interfaces.

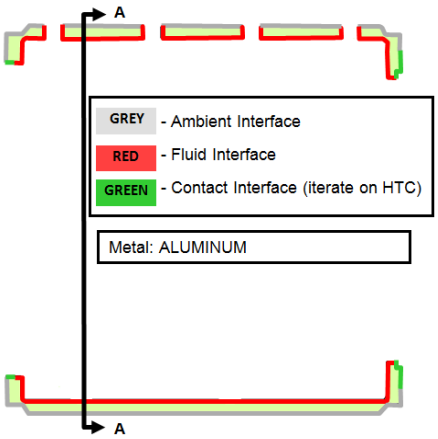

Figure 9. Coupling Guard Solid Domain Boundary Conditions.

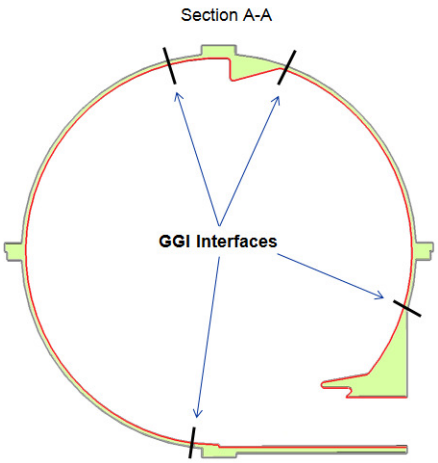

Figure 10. Solid Domain Boundary Conditions (View AA).

The convergence of the model was monitored by tracking the overall residuals (target <1e-04), the mass and energy imbalances (±0.1%), discrete monitors in the flow field (stable), and volume averaged quantities in the solid domains.

RESULTS -WITHOUT BOLTS

Case 2, with opening pressure of 14.6 psi (100.7 kPa), did not converge readily and was dropped without being completed. For cases 1 and 3, ingestion through the central outlet (Outlet 01 in Figure 11) was observed whereas Case 4, which lacked the central outlet, had no ingestion (Fig. 11-13). One should, however, keep in mind that these cases are without bolts. They clearly demonstrate that without the pumping action of the bolts, air can actually be ingested.

For Case 1, this ingestion flow is similar to that entering the system from each of the inlets. However, when the exit pressure is increased to 14.8 psi (102.0 kPa) (Case 3), all of the cooling flow entering the coupling guard comes from Outlet01. The CFX code creates artificial walls at the four inlets to prevent flow from leaving the model at an inlet.

Compared to Case 1, cooling flow is reduced by about 11.5% when Outlet01 is blocked off (Case 4). There is a large gap between the coupling guard and the rotating shaft (visible in Figure 14), creating a relatively low cavity pressure, which encourages ingestion in Cases 1 and 3. When Outlet01 is walled off (Case 4), flow recirculates in the region where the exit would be if it were not closed off.

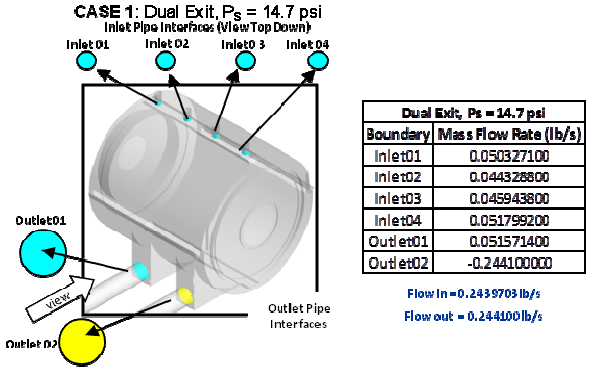

Dual Exit, Ps = 14.7 psi	
Boundary	Mass Flow Rate (lb/s)
Inlet01	0.050327100
Inlet02	0.044328800
Inlet03	0.045943800
Inlet04	0.051799200
Outlet01	0.051571400
Outlet02	-0.244100000

Flow In = 0.243970300 lb/s
Flow out = 0.244100 lb/s

Figure 11. Boltless Case 1.

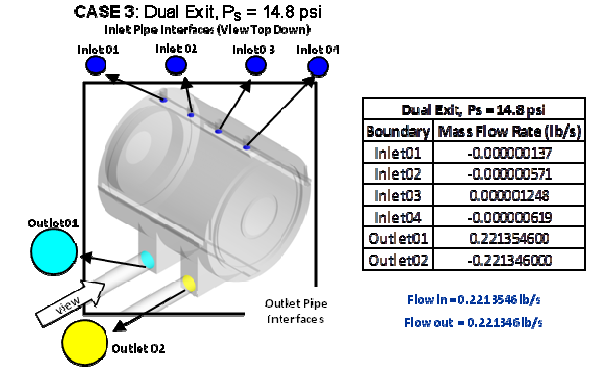

Dual Exit, Ps = 14.8 psi	
Boundary	Mass Flow Rate (lb/s)
Inlet01	-0.000000137
Inlet02	-0.000000571
Inlet03	0.000001248
Inlet04	-0.000000619
Outlet01	0.221354600
Outlet02	-0.221346000

Flow In = 0.221354600 lb/s
Flow out = 0.221346 lb/s

Figure 12. Boltless Case 3.

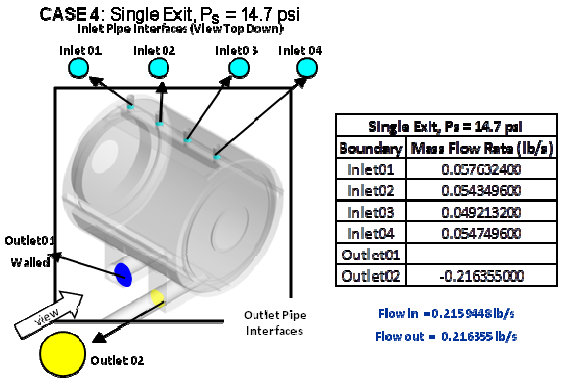

Single Exit, Ps = 14.7 psi	
Boundary	Mass Flow Rate (lb/s)
Inlet01	0.057032400
Inlet02	0.054349600
Inlet03	0.049213200
Inlet04	0.054749600
Outlet01	
Outlet02	-0.216355000

Flow In = 0.215944800 lb/s
Flow out = 0.216355 lb/s

Figure 13. Boltless Case 4.

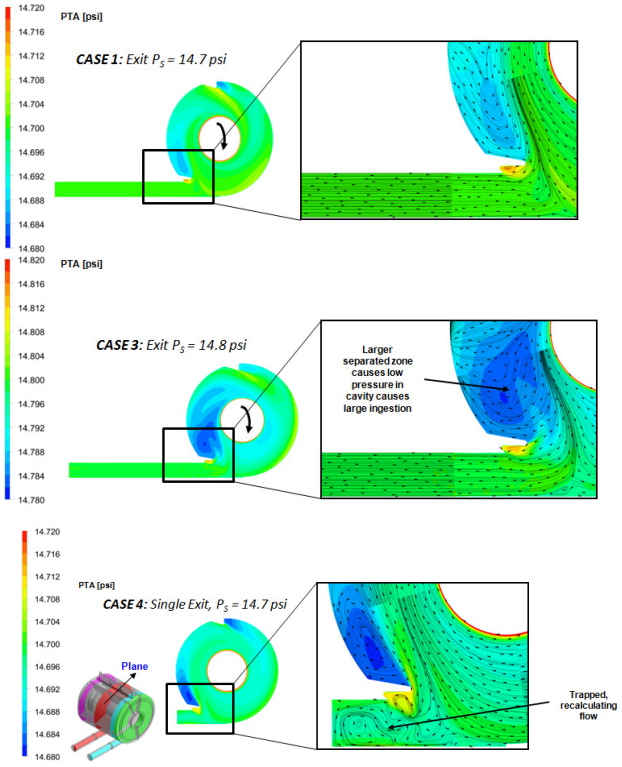

Figure 14. Absolute Total Pressure Contours through Outlet01.

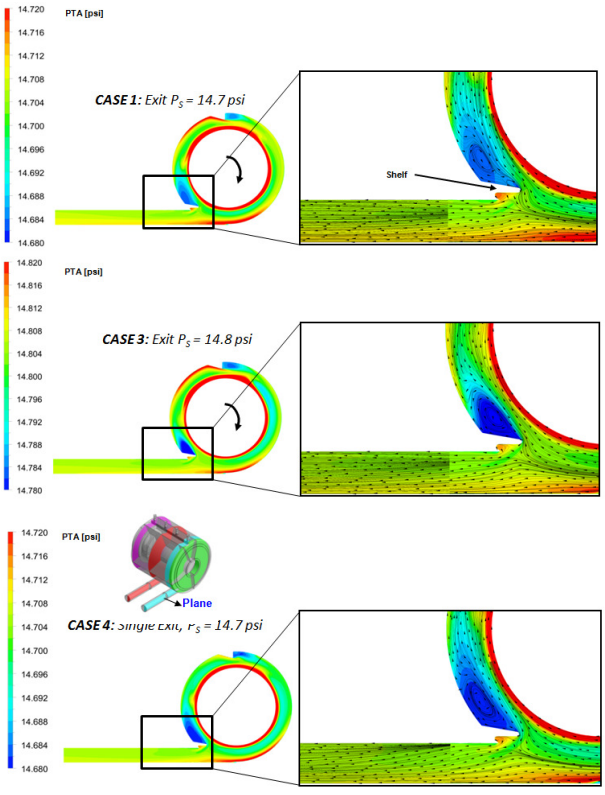

Figure 15. Absolute Total Pressure Contours through Outlet02.

The total pressure contours through the exhaust near the end, Outlet02 (Fig. 15), indicate that the shelf forms a smaller gap between the coupling guard wall and rotating shaft in all cases, which keeps the pressure near the exhaust high and flow pumping out of the system.

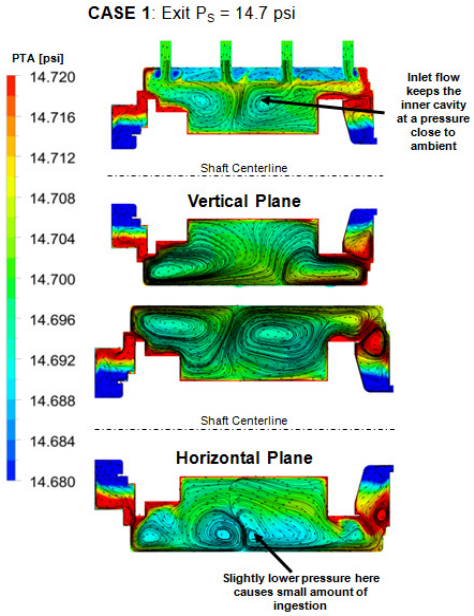

Figure 16. Absolute Total Pressure Contours (Case 1).

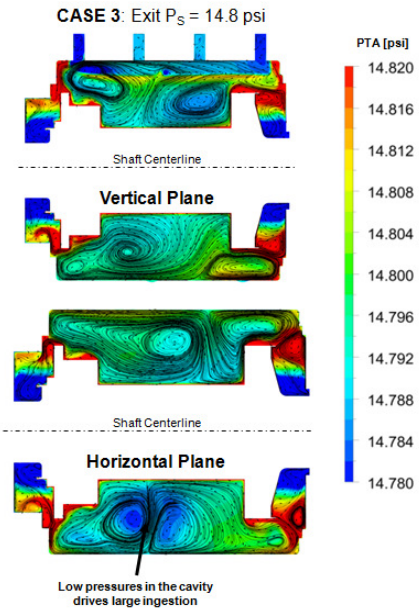

Figure 17. Absolute Pressure Contours (Case 3).

Total pressures on vertical and horizontal slices through the fluid domains (Fig. 16-19) exhibit lower pressures in the central cavity for Case 3 compared to either of the 14.7 psi (101.4 kPa) exit pressure cases. This lower pressure helps to drive the ingestion in Case 3.

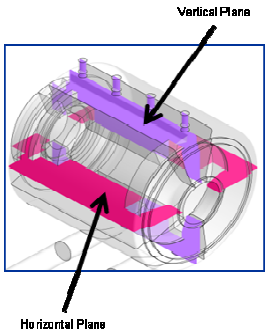

Figure 18. Position of the Planes.

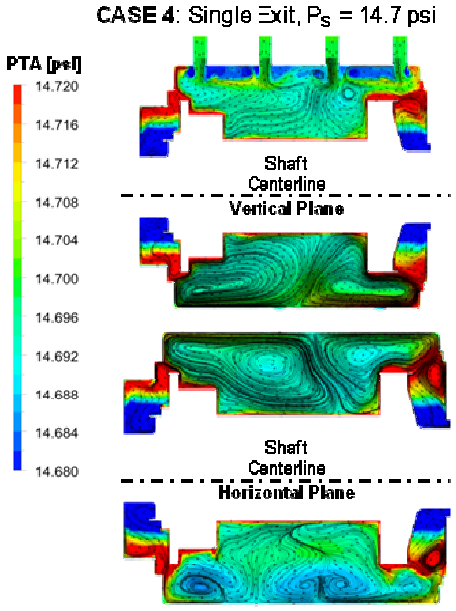

Figure 19. Absolute Pressure Contours (Case 4).

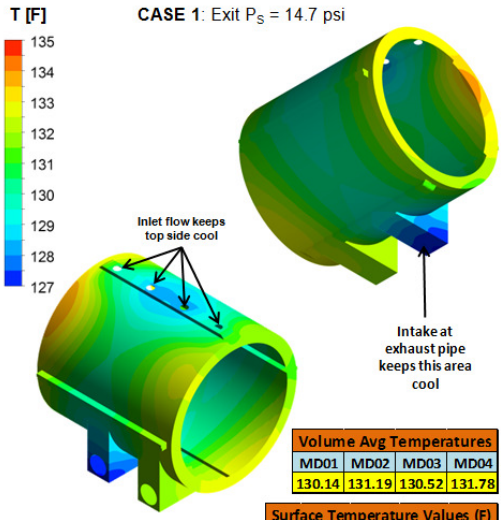

Volume Avg Temperatures			
MD01	MD02	MD03	MD04
130.14	131.19	130.52	131.78

Surface Temperature Values (F)				
	MD01	MD02	MD03	MD04
Min	127.94	128.64	126.84	129.25
Avg	130.09	130.87	130.49	131.50
Max	133.71	133.08	132.95	134.26

Figure 20. Metal Temperature Contours (Case 1).

The predicted metal temperatures in Figures 20-22 are much lower than the temperatures measured in the field. Hence, the model without bolt heads does not accurately represent the field conditions.

These results imply that a "perfect" bolt-head windage reduction feature might lead to lower temperatures than those observed in the field. Before drawing this conclusion, however, we wanted to verify that the model with bolt heads could predict the observed temperatures with reasonable accuracy.

The next section presents the setup and results of the cases with bolt heads included on the coupling flanges.

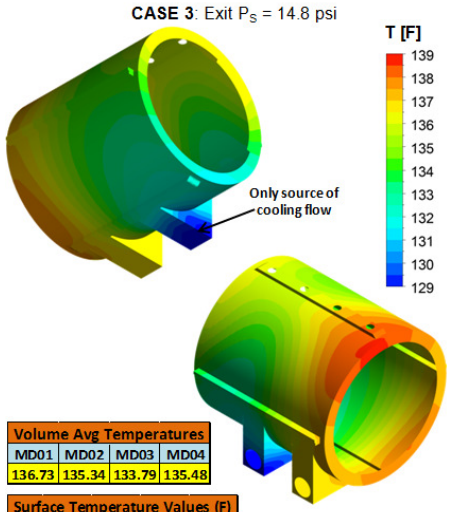

Volume Avg Temperatures			
MD01	MD02	MD03	MD04
136.73	135.34	133.79	135.48

Surface Temperature Values (F)				
	MD01	MD02	MD03	MD04
Min	135.11	132.19	127.97	132.18
Avg	136.72	135.24	133.71	135.33
Max	138.59	138.30	137.85	138.57

Figure 21. Metal Temperature Contours (Case 3).

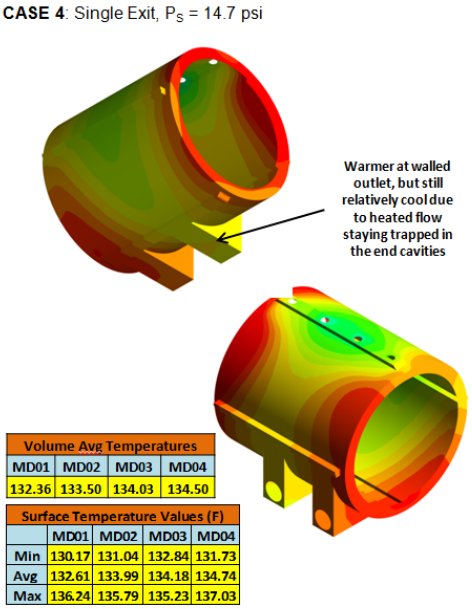

Volume Avg Temperatures			
MD01	MD02	MD03	MD04
132.36	133.50	134.03	134.50

Surface Temperature Values (F)				
	MD01	MD02	MD03	MD04
Min	130.17	131.04	132.84	131.73
Avg	132.61	133.99	134.18	134.74
Max	136.24	135.79	135.23	137.03

Figure 22. Metal Temperature Contours (Case 4).

CFD MODEL SETUP WITH BOLTS

The bolts were modeled as cylinders having diameters equal to the largest diameters of the bolt heads or nuts (Fig. 23). Due to the non-axisymmetric nature of the bolt features, the domain setup was modified to include a cylindrical domain split (Fig. 24) to accommodate an inner fluid domain set in the rotating frame of reference. Further, to minimize the number of interfaces, the angular domain splits were discarded in favor of full 360° domains. Locations of boundary conditions and interfaces are shown in Figures 24 and 25.

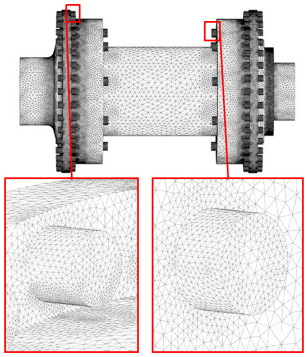

Figure 23. Surface Mesh for Cases with Bolts.

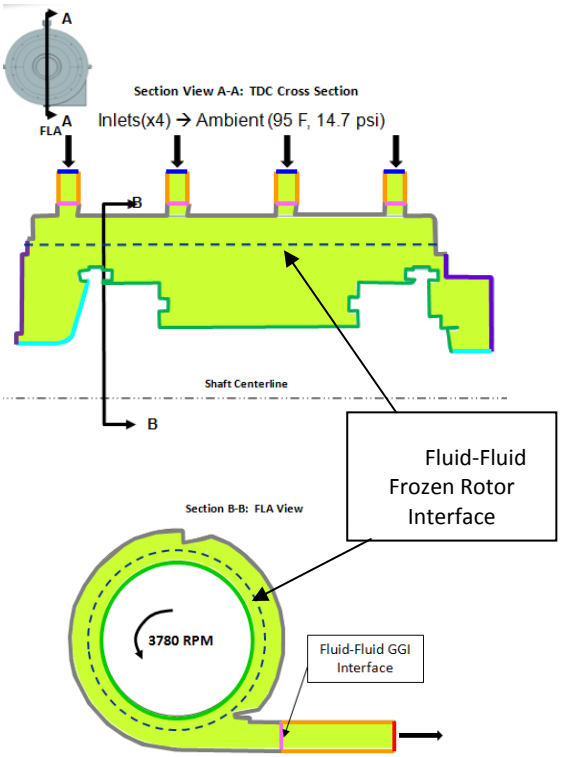

Figure 24. Boundary Conditions – Case with Bolts.

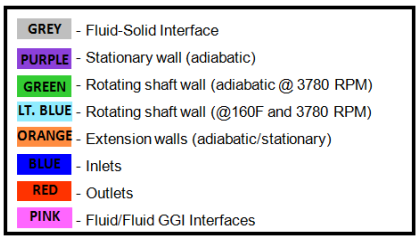

Figure 25. Key to Boundary Colors Used in Figure 24.

The first case that was analyzed with bolts (Case 5) was similar to Case 4 as given in Table 1. The inlet conditions were maintained as before. But to simulate the original field scenario, the central outlet port was removed as shown in Figure 26, and the exit pressure was set to 14.75 psi (101.70 kPa) to simulate resistance to exhaust air flow. Metal boundary conditions were identical to the cases without bolts. Case 5 served as a new baseline for cases with bolts.

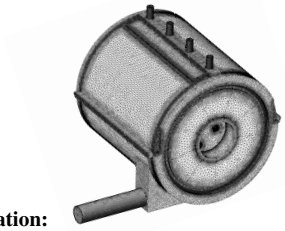

Mesh Information:
Number of Nodes: 9.8 million
Number of Elements: 33.3 million
Wall Clustering: Initial Cell Height: 1.5 x 10^{-4} (inch)

Figure 26. Domain with Bolts.

RESULTS WITH BOLTS - FIRST CASE

Compared to the boltless Case 4 from the earlier section, the first case with bolts showed almost 70% imore mass flow (0.367 vs. 0.216 lbm/s) (0.166 vs. 0.098 kg/s) (Fig. 27). Despite the additional mass flow in the system, volume average metal temperatures rose by approximately 70°F (40°C) compared to boltless Case 4 (~207°F vs. ~134°F) (~97°C vs. ~57°C).

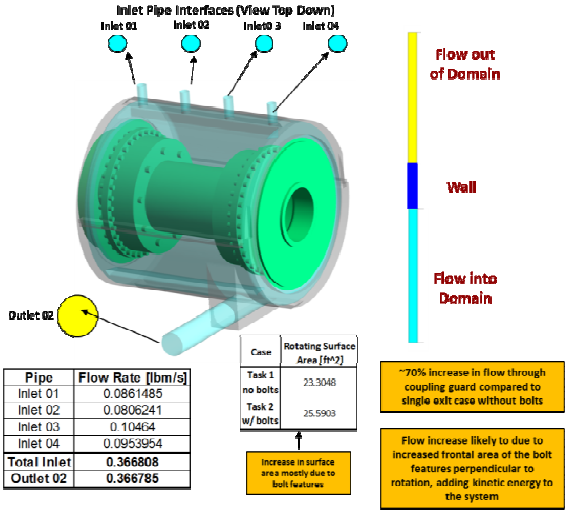

Figure 27. The First Case with Bolts (Case 5).

Clearly, the bolts provide a pumping action to drive the flow through the guard, as well as windage which imparts additional work to the fluid, and resulting in increased fluid temperature and guard metal temperature (Fig. 28). More important, the predicted temperatures are very close to the ones observed in the field (Table 2).

Table 2. Field Data vs. CFD Predictions.

Method	Temperatures (°F)	
	Average Metal	Maximum
Case 5 (CFD)	209	225.7
Field Data	219 to 222	

The maximum metal temperature was observed at the expander end of the coupling guard, which is furthest away from the outlet port.

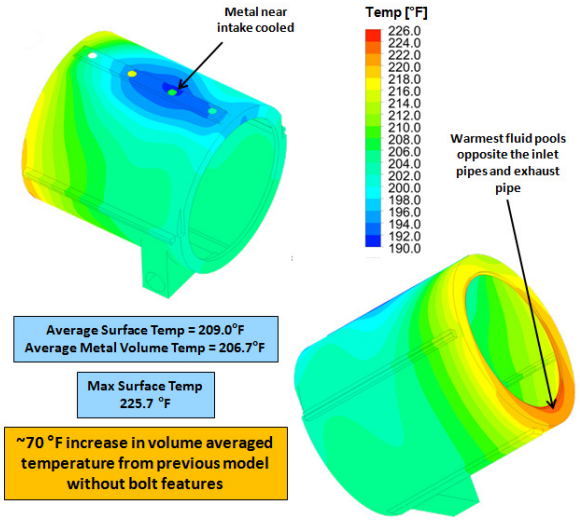

Figure 28. Temperature Contours (Case 5).

Internal fluid stream tubes (Fig. 29) illustrate the fluid warming quickly upon entering the system and rapidly being swirled out of the cavity, with very little flow reaching the end of the cavity furthest from the outlet. The fluid remaining in the cavity is continuously worked on by the rotating shaft and heated.

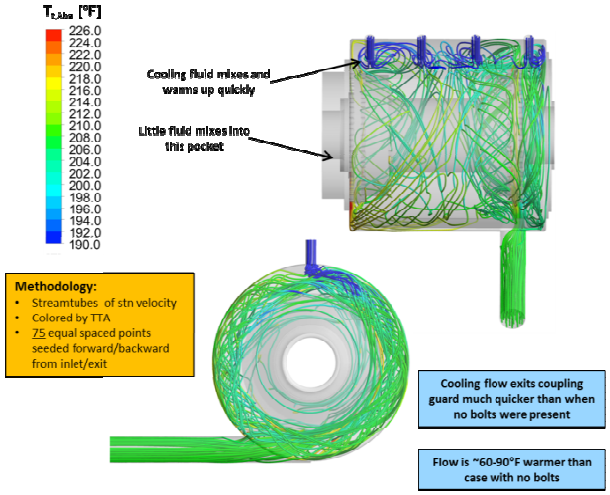

Figure 29. Streamtubes (Case 5).

Contours of absolute Mach number on various slices through the domain show significant increases near regions where the bolts were added (Fig. 30). Additionally, the pockets at each end of the cavity reflect the higher Mach number where the fluid is continuously worked on.

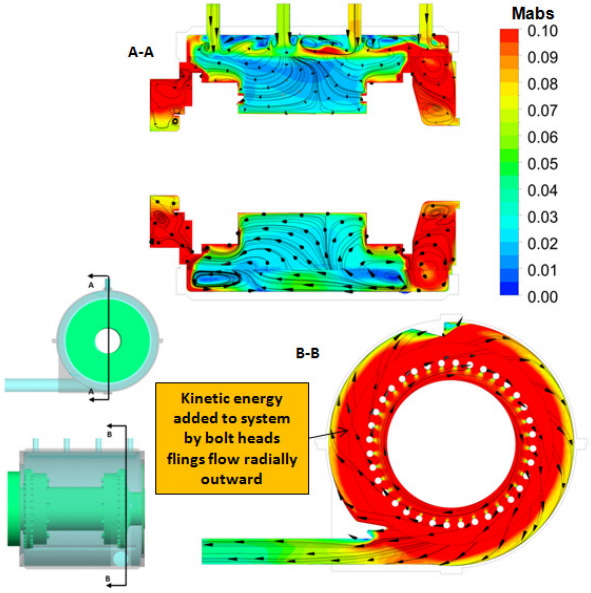

Figure 30. Absolute Mach Number Contours (Case 5).

Further evidence of the increased kinetic energy imparted to the fluid by the bolts can be seen in the contours of swirl and total pressure through the coupling guard cavity (Fig. 31 and 32). High values of these parameters in the pocket at each end of the coupling guard indicate that the fluid is continuously being worked on by the rotating hardware.

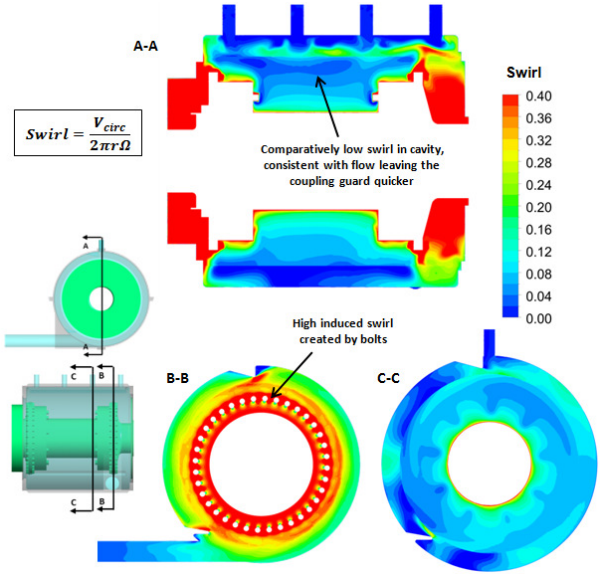

Figure 31. Swirl Contours (Case 5).

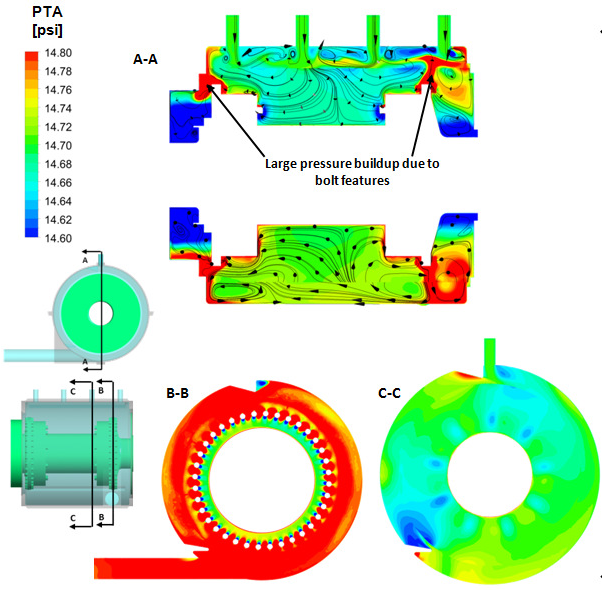

Figure 32. Total Pressure Contours (Case 5).

In the cases without bolts, both ends of the coupling guard heated up relatively evenly (i.e. the lengthwise variation of temperature was not as drastic as noted in the cases with bolts). However, when bolt features were added, the end furthest from the exhaust pipe experienced the highest surface temperature, as seen from the total temperature contours on various slices through the coupling guard (Fig. 33). At this end, the gap between the shaft components and the stationary walls is tighter than at the opposite end. The bolt heads close the gap further and pinch off the cavity, essentially trapping flow in this end where it is continuously worked on by friction from the bolt features.

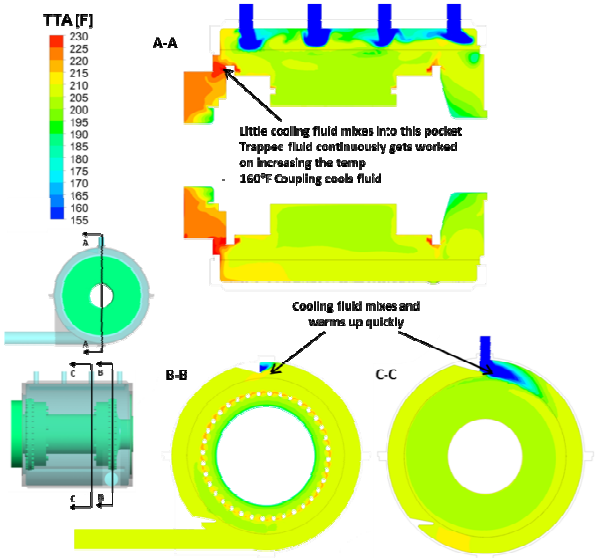

Figure 33. Total Temperature Contours (Case 5).

Here, the small gap separating the shaft and coupling guard at the side furthest from the exhaust can be clearly seen. In reality, the gap is even smaller, since these slices do not cut through bolts. The fluid temperatures are significantly higher in this region. Also, the 160°F (71°C) shaft absorbs heat and cools the flow. The same is true for all subsequent bolt cases. The opposite trend was noted in all cases without the bolts.

MORE CASES WITH BOLTS

Since one of the objectives behind this work was to mitigate the heating problems, CFD simulations were run with various combinations of parameters (Table 3).

Table 3. Cases for Models with Bolts.

Case #	Exit Static Pressure (psi)	# of Inlets	# of Outlets	Outlet Location	Outlet Area (in2)
5	14.750	4	1	End	15.9
5a	14.654				
5b	14.600				
6a	14.654		1	Center	
6b	14.600				
7a	14.654	2			
7b	14.600	2			
8	14.654	4	2	Ends	31.8

An increase in the cooling mass flow could provide a good reduction in the guard temperature. One way to achieve this was by reducing the exit static pressure. This would be easy to implement in the field due to ready availability of vacuum of about 1.5" (38.1 mm) of oil. This would give an outlet pressure of 14.654 psi (101.04 kPa). Additionally, cases were run with 14.6 psi (100.66 kPa) exit static pressure to see how it would affect the mass flow through coupling guard.

The configurations were also varied geometrically. Cases 5a and 5b (Fig. 34) compared with 6a and 6b (Fig. 35) showed

the effect of location of the outlet port. Cases 6a and 6b were also important for comparing with 7a and 7b. Cases 7a and 7b (Fig. 36) eliminated the middle two inlet ports and increased the size of the remaining inlet ports to maintain the same total flow area. This was intended to force flow to pass through more of the coupling guard volume rather than short-circuiting from the middle inlet ports to the center outlet port. After advantages were seen with the outlet port near the end rather than the center, Case 8 (Fig. 37) was created to see whether this advantage could be magnified with two end ports.

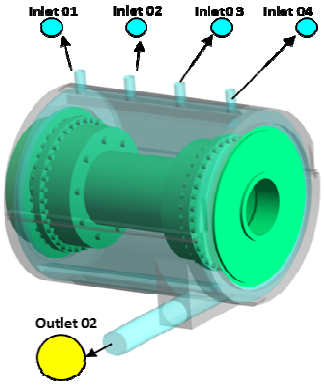

Figure 34. Cases 5, 5a, and 5b: End Outlet.

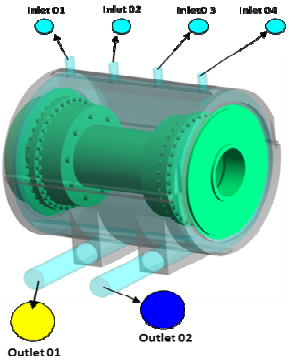

Figure 35. Cases 6a, 6b: Central Outlet (End outlet (in blue) was blocked).

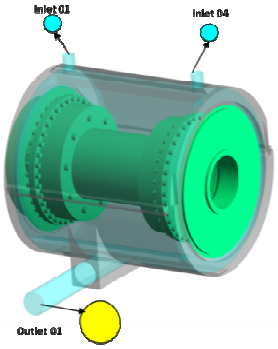

Figure 36. Case 7: Two Inlets and Central Outlet.

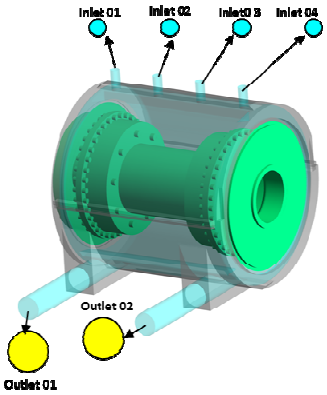

Figure 37. Case 8: Two End Outlets.

RESULTS WITH BOLTS - MORE CASES

For two sub-atmospheric boundary conditions, a substantial 35% increase in the flow was observed in the comparable geometries (Table 4).

Table 4. Effect of Exit Static Pressure on Mass Flow.

Case	Exit Static Pressure	Mass Flow Rate (lbm/s)	% change
5	14.750	0.367	-
5a	14.654	0.495	34.87
5b	14.600	0.497	35.42

The effect on the temperature was also substantial (Table 5).

Table 5. Effect of Exit Static Pressure on Temperature.

Case	Exit Static Pressure	Temperature (°F)	
		Average Metal Volume	Max Surface
5	14.750	206.70	225.70
5a	14.654	188.10	204.70
5b	14.600	181.50	197.80
6a	14.654	197.00	216.00
6b	14.600	185.00	200.90

The positioning of outlet ports, the number of inlets, and the exit static pressure had direct effects on the amount of cooling flow through the coupling guard, and consequently on the coupling guard temperature.

Compare, for example Cases 5a and 6a, where the single outlet port was moved from the end to the center . The exit static pressure was set to 14.654 psi (101.031 kPa), and other boundary conditions remained the same. Surface temperatures are shown in Figures 38 and 39 and in Table 6.

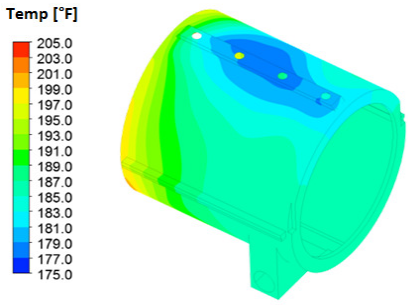

Figure 38. Case 5a with End Outlet Port.

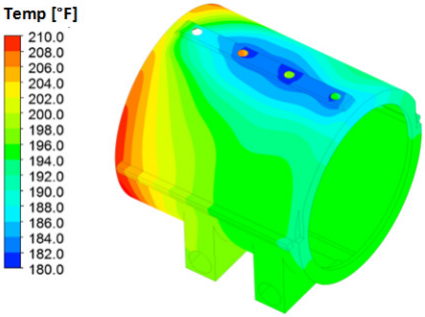

Figure 39. Case 6a with Central Outlet Port.

Moving the port location reduces mass flow from 0.495 lbm/s to 0.416 lbm/s (0.224 kg/s to 0.188 kg/s), a 15.96% reduction. This increases the maximum surface temperature from 204.7 °F to 216.0°F (95.9°C to 102.2°C); an 11.3°F (6.3°C) increase. Similar trends are observed in Cases 5b and 6b (Fig. 40 and 41).

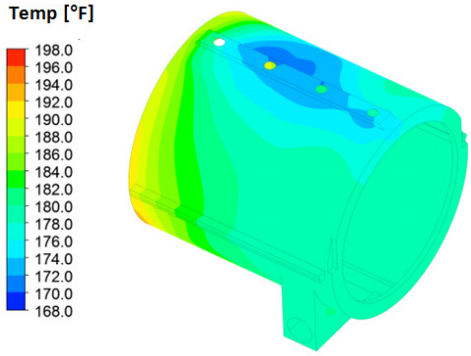

Figure 40. Case 5b with End Outlet and 14.600 psi (100.658 kPa).

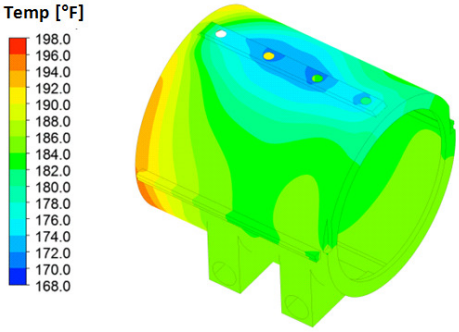

Figure 41. Case 6b with Central Outlet and 14.600 psi (100.658 kPa).

Table 6. Effect of Port Location.

Case	Exit Static Pressure	Temperature (°F)	
		Average Metal Volume	Max Surface
5a	14.654	188.10	204.70
6a		197.00	216.00
5b	14.600	181.50	197.80
6b		185.00	200.90

For Cases 7a and 7b, the number of inlets was reduced to two, but the total area was maintained. The same center exit port as in Cases 6a and 6b was used. This configuration was intended to improve the effectiveness of the limited cooling flow by forcing it through more of the coupling guard volume. Results from Cases 7a and 7b are shown in Table 7.

Table 7. Cases 7a and 7b.

Case	Exit Static Pressure	Temperature (°F)		Mass Flow (lbm/s)
		Average Metal Volume	Max Surface	
7a	14.654	226.9	249.2	0.279
7b	14.600	210.2	231.2	0.354

Despite the fact that the total inlet flow area remained the same, the flow rate was reduced from 0.416 (Case 6a) to 0.279 lbm/s (0.188 to 0.127 kg/s), a 32.93% reduction. Temperatures rose compared to the corresponding Cases 6a and 6b.

The reduced mass flow had a stronger detrimental effect than the benefit from forcing the flow through more of the coupling guard volume. Clearly, the location of the inlet ports is of great importance, and not just the through flow area.

This can also be seen in Figure 42, where the cooling flow from the two middle inlets is not mixing with the flow in the cavity to reduce the temperatures. Case 7a (Fig. 43) magnifies the problem by directing even less inlet flow toward the center. Cases 6b and 7b show the same trend (Fig. 44). Note that the stream tubes are of the velocity in stationary frame, colored by total temperature and generated by seeding points in the forward and backward directions at each inlet and exit.

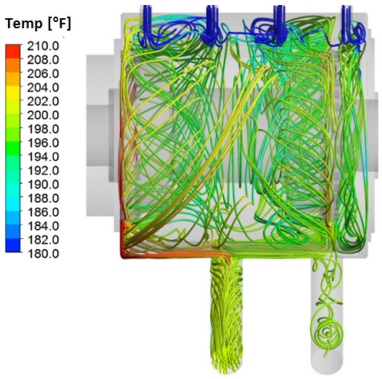

Figure 42. Case 6a: Exit Static Pressure=14.654 psi (101.031 kPa).

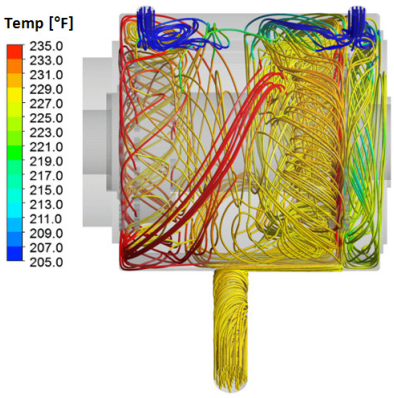

Figure 43. Case 7a: Exit Static Pressure=14.654 psi (101.031 kPa).

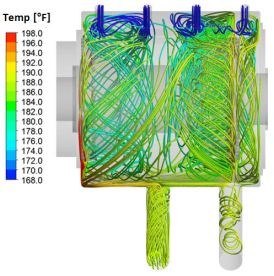

Case 6b: Exit Static Pressure=14.600 psi (100.658 kPa)

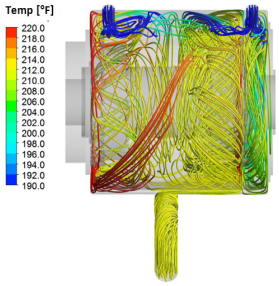

Case 7b: Exit Static Pressure=14.600 psi (100.658 kPa)

Figure 44. Case 6b vs. 7b.

From Figures 45 and 46, it is easy to notice the non-uniform distribution of the temperature along the longitudinal axis of the coupling guard. This has to do with clearances available on each end of the coupling, and is explained later.

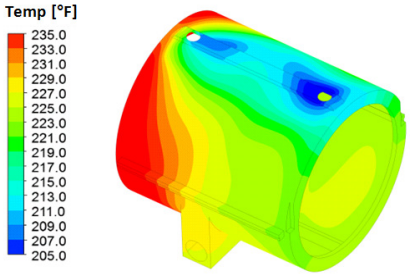

Figure 5. Case 7a: Two Inlets, Central Outlet.

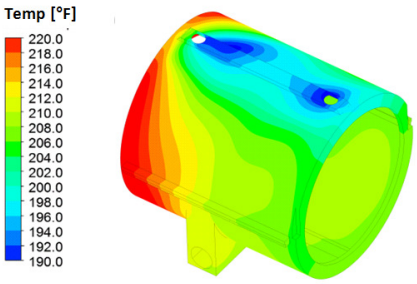

Figure 6. Case 7b: Two Inlets, Central Outlet.

In Case 8, two exhaust ports were modeled tangential to and axially aligned with the coupling flanges, as shown in Figure 37.

The temperature contour plot for this case is shown in Figure 47. This case has the highest mass flow through the coupling guard and lowest surface temperature. Compared to Case 5, Case 8 has approximately 52.86% more flow, and 36.6°F (20.3°C) lower maximum surface temperature. Case 8 appears to be the best arrangement so far.

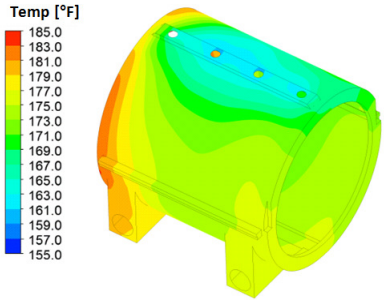

Figure 42. Case 8: Axially Aligned Outlet Ports.

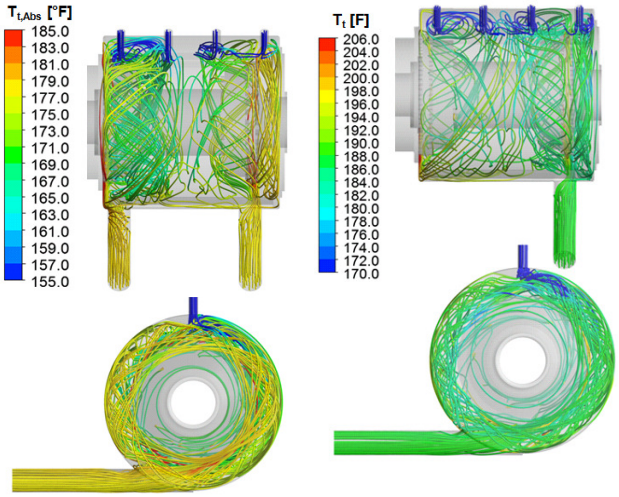

Case 8 Case 5

Figure 43. Streamtubes of Velocity in Stationary Frame.

Table 8 and Figure 49 show the summary of the cases analyzed so far.

Table 8. Summary of Results.

Case	Temperature (°F)		Mass Flow Rate (lbm/s)
	Average Metal Volume	Max Surface	
5	206.70	225.70	0.367
5a	188.10	204.70	0.495
5b	181.50	197.80	0.497
6a	197.00	216.00	0.416
6b	185.00	200.90	0.497
7a	226.90	249.20	0.279
7b	210.20	231.20	0.354
8	174.80	189.10	0.561

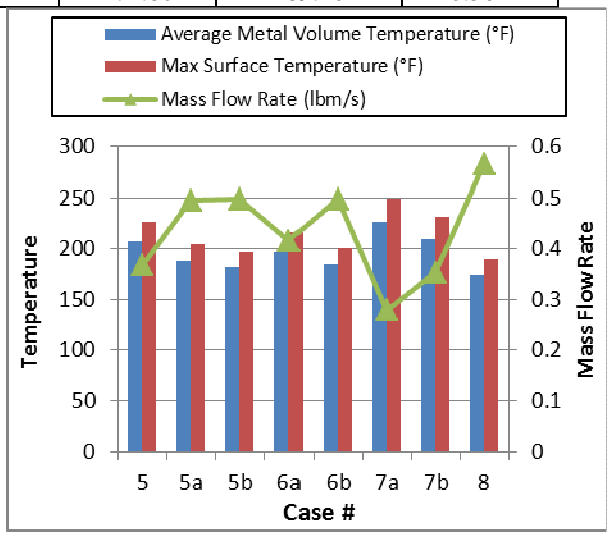

Figure 44. Temperature and Mass Flow Rate Through Coupling Guard.

As noted previously, the temperature along the coupling guard was not uniform. Notice that in Figure 50, the temperatures at one end are much higher.

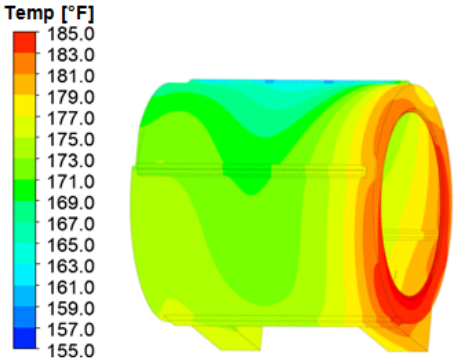

Figure 45. Case 8 Rear View.

In Figure 51, the fluid in the left corner of the coupling guard receives very little cooling flow due to tight clearances between the coupling and the stationary walls. This indicates that larger clearances, greater volume, and possibly breather tubes should be provided.

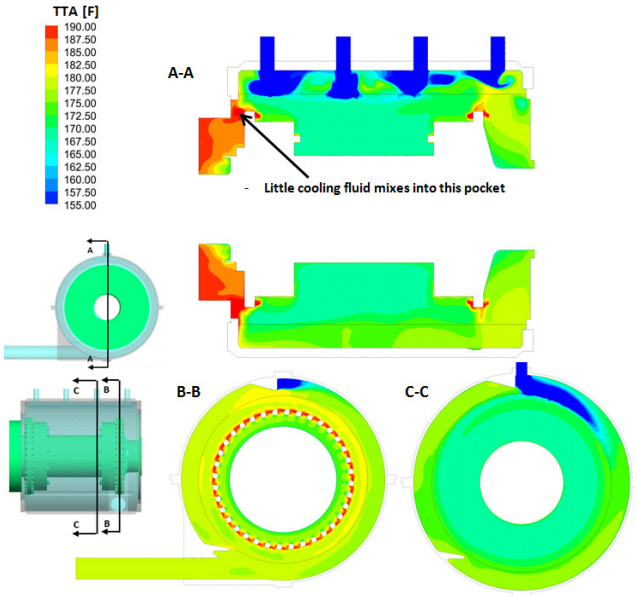

Figure 46. Case 8 Total Temperature Distribution.

CONCLUSIONS

The results presented here are far from a thorough parametric study to derive an exact methodology for coupling guard design. The following, however, can be concluded.

- A CFD model of a rotating coupling inside a stationary coupling guard must include bolt and nut geometry to effectively predict coupling guard heating, temperature, and flow. A model without the bolts, using only smooth surfaces, predicts very little heating.
- A single horizontal tangential discharge at the bottom axial center of the coupling guard has little pumping action. Horizontal tangential discharges at the

bottom in approximate alignment with the rotating coupling flanges improve pumping action and increase mass flow through the coupling.

- A coupling guard with one axially centered horizontal tangential discharge nozzle operating in parallel with a second horizontal tangential discharge nozzle in line with a rotating coupling flange can create flow recirculation from the discharge nozzle at the coupling flange back into the coupling guard through the discharge nozzle at the axial centerline.
- Coupling guard volumes that are isolated by close clearances between the rotating coupling and the guard inside diameter and that do not have an air inlet will have the highest heating and temperature because of limited cooling flow.
- When total flow area is equal, a larger number of smaller diameter inlet air breathers spaced along the top of the coupling guard provides a more effective cooling air inlet than does a reduced number of breathers of larger diameters.
- Air flow through the coupling guard can be increased significantly by reducing discharge vent pressure by only a few inches of water. In the present work, a 35% mass flow increase was seen by reducing exit pressure by only 1.3" (38.1 mm) water pressure. Clearly, the mass flow rate is very sensitive to exit static pressure.
- Adding a high efficiency coalescing filter at the coupling guard discharge vent effectively eliminates oil misting but increases discharge static pressure due to the coalescing filter pressure loss.

Coupling Guard Design Recommendations:

- Locate fluid exits tangential to coupling flanges having bolt heads.
- Equally distribute, along the coupling guard axis, a reasonably greater number of small area inlet breathers rather than a small number of large area inlet breathers.
- Make the clearance between the coupling guard inside diameter and the coupling flanges as large as possible, while considering installation constraints.
- Avoid creating isolated high temperature internal volumes by using large internal radial clearances and increasing the axial distance between the coupling flanges and the ends of the coupling guard.
- Consider applying forced ventilation by creating a vacuum at the coupling guard fluid exits.
- Take “system” approach to designing a guard. Consider other elements in the piping system, and how they affect the air flow through the guard.

Computational Modeling Recommendations:

- Consider using a 360° domain instead of a sector for more realistic analysis
- Model bolt-heads to accurately simulate the heat generation due to windage

Clearly, in order to arrive at reasonable correlation between the field data and computational model, a more detailed parametric study is necessary.

REFERENCES:

API 671/ISO 10441:2007, 2007, “Special Purpose Couplings for Petroleum, Chemical and Gas Industry Services,” Fourth Edition, American Petroleum Institute, Washington, D.C.

Calistrat, M. M. and Munyon, R. E., 1985, “Design of Coupling Enclosures”, Proceedings of Fourteenth Turbomachinery Symposium, Turbomachinery Laboratory, Texas A & M University, College Station, pp. 51-57.

Calistrat, M. M., 1990, “Recent Case Histories With Coupling Enclosures”, Proceedings of Nineteenth Turbomachinery Symposium, Turbomachinery Laboratory, Texas A & M University, College Station, pp. 37-42.

Carter, D., Garvey, M., Corcoran, J. P., 1994, “The Baffling and Temperature Prediction of Coupling Enclosures”, Proceedings of the Twenty-third Turbomachinery Symposium, Turbomachinery Laboratory, Texas A & M University, College Station, pp. 115-123.

Pennington S., Meck K., 2012, “Effectiveness of Windage Features on High Speed Couplings”, Proceedings of the Forty-first Turbomachinery Symposium, Turbomachinery Laboratory, Texas A & M University, College Station.

ACKNOWLEDGEMENTS

We’d like to thank Elliott Group for allowing us to publish and present this work.